Songklanakarin J. Sci. Technol.
44 (2), 289-295, Mar. - Apr. 2022

http://www.sjst.psu.ac.th

Original Article

Quasi-one-dimensional graphene structure: Study of finite bandgap and effective mass with width

Monika Khetarpal*

Department of Physics, Government Dungar College, Bikaner, 334001 India

Received: 19 June 2021; Revised: 13 August 2021; Accepted: 19 August 2021

Abstract

A tight-binding approach comprising a p_z orbital basis set is employed to induce a bandgap in massless Dirac Fermion, graphene. The role of the structural parameter, chirality, has been explored to determine the electronic band structure of armchair graphene nanoribbon (AGNR). The present results show that the key parameter, the bandgap in quasi-one-dimensional graphene nanoribbon, arises from quantum confinement. It is observed that the total number of carbon atoms present in the overall unit cell of AGNR is equal to the total number of subbands in the corresponding electronic structure. Important band structure parameter effective mass is computed from the parabolic region of the band structure. A decreasing trend of energy bandgap and effective mass as a function of width has been reported. Our results demonstrated that armchair graphene nanoribbon can be divided into three families 3p, 3p+1, and 3p+2, p is an integer. In addition, the electronic density of states at different chirality values has been studied, to support our findings of the electronic band structure.

Keywords: AGNR, electronic band structure, effective mass, nano-ribbon width

1. Introduction

Graphene nanoribbon (GNR), a planar, finite, and quasi-one-dimensional graphene structure constitutes a class of fast developing innovative attractive materials (Sahu & Rout 2017; Senkovskiy *et al.*, 2021; Wang, Zhao, Yang & Liu 2013). Unconstrained graphene is a two-dimensional one-atom-thick carbon layer with carbon atoms arranged in a honeycomb lattice. Theoretical investigation of graphene's linear and non-linear optical absorption properties reveals its application in optical and optoelectronic devices (Mu & Sun, 2020; Mu, Chai, Wang, & Li, 2019). Graphene and related materials are strong candidates for photodetectors, surface plasmon waveguides, metamaterials, and nanolasers in the future (Cui, Wang & Sun 2021). It exhibits a peculiar linear dispersion around the Dirac point and has zero bandgap (Raza & Kan 2008). The behavior of charge carriers in graphene is just like massless Dirac Fermions (Sheka 2018).

Since graphene does not have a bandgap it cannot be used in logic devices. Countless approaches have been developed to engineer a bandgap in graphene. GNR is a structure obtained from a graphene sheet in a particular orientation. GNR with narrow width of less than 10 nm are promising materials as they have a wide range of spectrum of application to be used as sensors (Shrivastav, Cvelbar & Abdulhalim, 2021), conductive films (Ray, Parmar, Date & Datar 2021), batteries (Jaramillo-Quintero *et al.*, 2021), energy conservation/storage devices (Wieland, Li, Rust & Chen, 2021; Ghosh, Sarkar, Devi & Kim, 2021). GNR has been classified as a zigzag (ZGNR) and armchair (AGNR) depending on the alignment of edge atoms (Wakabayashi, Sasaki, Nakanishi & Enoki 2010). A vast number of studies (Jhamb, Kamal, Randhawa & Sharma 2015; Kim *et al.*, 2018; Poklonski, Kislyakov, Vyrko & Bubel 2012; Dubois, Zanolli, Declerck & Charlier 2009) of these edge structures have been made because the electronic and magnetic properties of GNRs depend on them.

Numerous efforts have been made to fabricate atomically precise GNRs, which incorporate top-down or bottom-up approaches (Houtsma, Rie & Stohr 2021; Yang, Lucotti, Tommasini & Chalifoux 2016). Recent development shows that GNR can be synthesized by longitudinally unzipping carbon nanotube (Jun *et al.*, 2021; Kuzmany *et al.*, 2021). Solution dispersion, a chemical method (Shekhirev &

*Corresponding author
Email address: drmonikaphy7@gmail.com

Sinitskii 2017) has manifested that graphene sheets impulsively split into narrow ribbons comprisal of smooth edges.

Theoretical aspects using the tight-binding (TB) approach (Wang *et al.*, 2007; Yazyev 2013) or DFT approach (Ma, Guo, Xu & Chu 2012) reveal that, unlike graphene, AGNR can be either metallic or semiconducting. AGNR properties are controlled by the width of the nanoribbon and the crystallographic orientation of the edges or chirality (Nakada, Fujita, Dresselhaus & Dresselhaus 1996). Characteristics of the GNR are anomalous integer quantum hall effect, the ability to re-engineer electronic bandgap with the variation of carrier concentration, or by imposing an external electric field (Raza & Kan 2008).

It has been proven that the AGNR bandgap is larger than those of bilinear graphene under a vertical electrical field, making AGNR a promising candidate for the fabrication of FET devices (Chen, Sangai, Gholipour & Chen 2013). First-principle simulations indicated that the edge bond relaxation in AGNRs is a predominant parameter to determine their bandgap energies as the bonding characteristics between carbon atoms drastically change at the edges (Sako, Hosokawa & Tsuchiya, 2010).

The tight-binding method of modelling materials (Wang *et al.*, 2021; Goringe, Bowler & Hernandez, 1997) is a conventional, simple, and highly computational efficient tool for the quantitative description of electronic structures. Theoretically, another method such as density functional theory coupled with LDA has the disadvantage that it underestimates the bandgap of semiconductors and insulators (Miyake & Saito, 2005). The GW approximation of many-body perturbation theory is computationally extremely expensive (Wilhelm, Golze, Talirz & Hutter, 2018). Keeping this in mind, the molecular structure, electronic band structure, and effective mass of AGNR are computed using the tight-binding model. Small-width AGNR, due to the large bandgap, plays an important role in room-temperature electronics (Borin Barin *et al.*, 2019). Hence, the present study focuses on the investigation of the electronic structure of AGNR having a very small width in chirality ranging from (4, 0) to (15, 0). Experimentally manufacturing GNR in the range of 1-2nm has the drawback that line edge roughness due to lithography and etch process (Knoch, 2020) is transferred into fluctuating potential along the nanoribbon. This leads to discrepancies in the electronic properties. Compared to the experimental landscape, a lot of theoretical research work (Cassiano, Monteiro, de Sousa, & e Silva, 2020; Hayyu, Azhar & Majidi, 2018; Kheirabadi, Ghayour & Sanaee, 2020; Salih & Ayesh 2021; Xie *et al.*, 2015; Wilhelm *et al.*, 2018) has been done to elucidate the electronic structure of AGNR. But still, further study is needed to get a clear picture of the band structure of AGNR by taking edge bond relaxation effects into account. Along with this, previous findings have triggered me to investigate the shape of subbands, effective mass, and the role of bonding in AGNR. The nano hub online simulator tool CNT Band (Seol *et al.*, 2006) has been used for this purpose. This tool uses MATLAB programming scripts.

2. Theory

The electronic band structure of armchair edge graphene nanoribbon has been evaluated using the TB approach for the π electron network. s, p_x, and p_y orbitals are at a larger distance from the Fermi level, hence p_z orbital mode has been employed in this study. A p_z orbital overlapping integral t = 3 eV is adopted in our approach. By considering only the nearest neighbor interaction, the C-C bond length is constant with the value of $a_{c\text{-}c}$ = 0.142 nm. The length of the unit cell in AGNR in this TB simulation is 0.426 nm.

The energy dispersion of graphene near the Fermi points are Dirac cones because the band structure of graphene nanoribbons can be predicted from a 2D graphene sheet, which is a zero-gap semiconductor (Jia *et al.*, 2016). Dirac cone is created when the upper and lower bands cross at point K (K') in the Brillouin zone termed as Dirac points. The low energy dispersion relation at the Dirac point (Johari, Ahmadi, Chek & Amin 2010) can be represented by the massless Dirac equation

$$E(k) = \pm \frac{3ta_{c-c}}{2} \sqrt{\beta^2 + {k_x}^2} \quad (1)$$

here, β is the quantized wave vector and k_x is the wave vector in the direction of the length of the nanoribbon. Band energy expressed in Equation 1 can be rephrased as

$$E = \pm \frac{E_g}{2} \sqrt{1 + \frac{k_x^2}{\beta^2}} \quad (2)$$

where the energy bandgap of GNR is $E_g = 3ta_{c\text{-}c}\beta$. Equation 2 states that the relation between the energy and wave vector is not parabolic. For semiconducting GNR, a parabolic relation between energy and wave vector is built by adopting a square root approximation. Near Γ the energy-wave momentum relationship for carriers within the first Brillouin zone is

$$E = \frac{E_g}{2} + \frac{\hbar^2 k_x^2}{2m^*} \quad (3)$$

here, m^* is the effective mass of GNR.

3. Results and Discussion

3.1 Structural analysis

GNR has nomenclature zigzag and armchair, which is determined by the pattern that appears on their transport edge whereas carbon nanotube (CNT) is named based on pattern on the circumference (Li, Xu, Srivastava & Banerjee 2009). Both types of nanomaterials are described by chirality (n, m) and chiral angle θ defined as

$$\theta = \tan^{-1} \frac{m\sqrt{3}}{2n+m} \quad (4)$$

In Equation 4, when θ=0˚ the value of m is zero, hence an armchair edge GNR has chirality value n=integer and m=0. With the variation of index n in the chirality (n, 0) the width of armchair edge GNR also varies as

$$W = \frac{(N-1)}{2} \sqrt{3}\, a_{c-c} \quad (5)$$

In Equation 5, N depicts the number of dimer lines. Figures. 1(a) and 1(b) shows the representative model of AGNR for chirality (6, 0) and (13, 0) depicting the number of dimer lines along the width W. It is evident from Figures 1(a) and 1(b) that the number of dimer lines in (6, 0) and (13, 0) AGNR are 6 and 13, respectively. Therefore, it can be inferred that the total number of dimer lines N obtained in AGNR is equivalent to the first index n in chirality (n, 0).

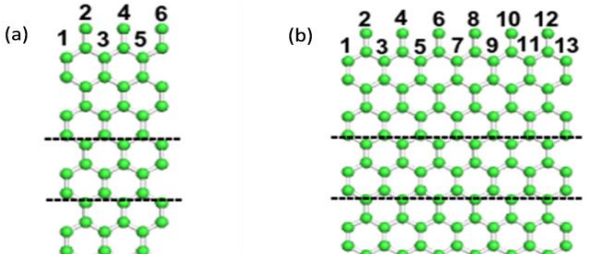

Figure 1. Structure of Armchair Graphene Nanoribbon showing the number of dimer lines along the width of the ribbon. The region between the dashed lines depicts the unit cell. (a) Chirality (6, 0), Dimer Lines (N=6), and no of carbon atoms in the unit cell (12). (b) Chirality (13, 0), Dimer Lines (N=13), and no of carbon atoms in the unit cell(26)

Consequently, in the present approach following the previous convention (Dubois, Zanolli, Declerck & Charlier 2009), we cite an AGNR comprising of N dimer lines as N-AGNR. The unit cells are shown in the Figures. 1(a) and 1(b) have 12 and 26 carbon atoms respectively for (6, 0) and (13, 0) AGNR. Hence it can generally be stated that the number of carbon atoms in the unit cell of AGNR is 2N.

3.2 Electronic band structure

The electronic structure of AGNR is computed using the p_z level of the TB theory, which shows that two-thirds of AGNR are semiconducting, and depending on the value of chirality (n, 0) other AGNR are metallic. Similar to CNT, GNR is both semiconducting and metallic (Wang *et al.*, 2007). Figures. 2 (a-l) depict the band structure of an armchair edge N-AGNR for N ranging from 4 to 15. The examination of Figure 2 shows that a bandgap can be generated near Dirac points of graphene. With an increase in the chirality of an AGNR by one the total number of the subbands increases by two. The total number of subbands in the band structure of AGNR is the same as the total number of carbon atoms present in their overall unit cell.

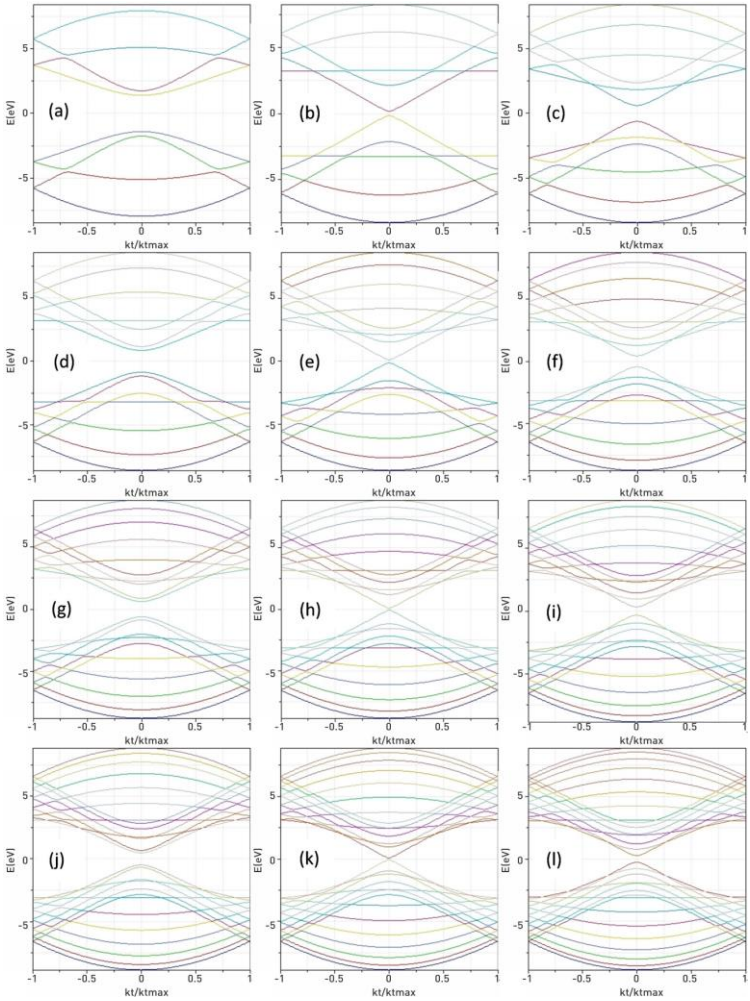

Figure 2. Band structure of AGNR. (a) N=4. (b) N=5. (c) N=6. (d) N=7. (e) N=8. (f) N=9. (g) N=10. (h) N=11. (i) N=12. (j) N=13. (k) N=14. (l) N=15

AGNR can be divided into three distinct families N = 3p, N = 3p+1, N = 3p+2, p is an integer. The top of the valence band and the bottom of the conduction band are located at K= 0. For family N = 3p and 3p+1, there exists a direct bandgap and these armchair edge GNR are semiconductors. As it is clear from Figures 2 (b), (e), (h), and (k) the system is metallic when N = 3p+2, even though it exhibits an infinitesimally small bandgap. The metallic character of the nanoribbon is enhanced with the increase in the width of the nanoribbon as the bandgap becomes almost zero at larger width. The variation of bandgap with width for these three distinct categories follows an inverse relation with the width and is depicted in Figure 3. Results are in agreement with the earlier reported results (Kheirabadi, Ghayour & Sanaee 2020; Son, Cohen & Louie, 2006). The three distinct families of armchair edge GNR follow a Gap size hierarchy, $\Delta_{3p+1} > \Delta_{3p} > \Delta_{3p+2}$. The semiconducting behavior of an AGNR can be attributed to quantum confinement. The bandgap calculated at Γ point in AGNR for three distinct groups is tabulated in Table 1(a) to Table 1(c).

Along with this, the shape of subbands is also an important key factor that affects the electronic properties of AGNR. Figures 2 (b), (e), (h), and (k) show that the energy subband at top of the valence band and bottom of the conduction band is linear for family N=3p+2. From Figure 2 it can be visualized that there is a parabolic dispersion around the Γ point, AGNR with family N = 3p having a steeper slope than those with the family N = 3p+1. Effective mass is calculated from the E-k dispersion curve near the parabolic regime. The creation of the bandgap in GNR leads to a massive Fermionic behavior of charge carriers. Therefore small bandgap (large bandwidth) GNR should have a lower effective mass.

In Figure 4, a plot of effective mass m^* in units of free electron mass m_0 with width is displayed for distinct families, the variation for the 3p and 3p + 1 family is plotted, and 3p + 2 family is not included as it exhibits linear dispersion relation. The effective mass of the charge carrier's hole and electron is taken to be the same. The variation of m^* shows it has a value ranging from $0.0769m_0$ to $0.492m_0$. The trend followed as observed in Table 2 (a) and Table 2(b) is $m^*(3p+1) > m^*(3p)$, for all p values. This behavior can be subjected to the cutting scheme in graphene to produce GNR, the cut closer to the Dirac point will result in a conic section that is sharper and hence will lead to the lower effective mass of charge carriers (Tayo 2014).

Using the p_z orbital approach the plots of the dependence of the density of states against the energy of the three families 3p, 3p+1, and 3p+2 are displayed in Figures. 5(a-l).

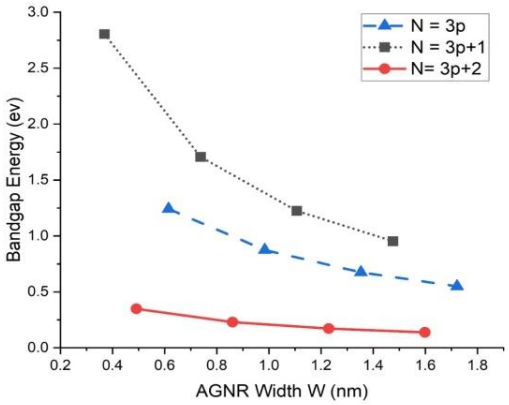

Figure 3. Energy Bandgap as a function of ribbon width for distinct families of AGNR

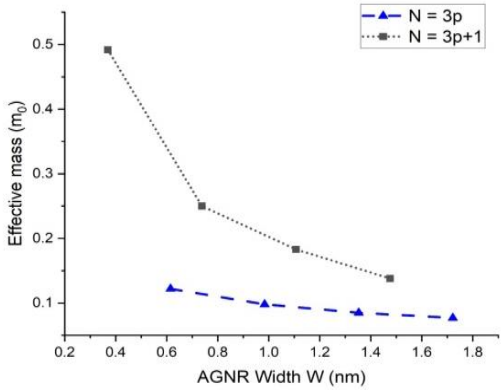

Figure 4. Effective mass as a function of ribbon width for distinct families of AGNR

Table 2. (a) Effective mass v/s width for family N= 3p, where p lies in [2, 5], (b) Effective mass v/s width for family N= 3p+1, where p lies in [1, 4]

a		b	
Width W (nm)	Effective mass (m_0)	Width W (nm)	Effective mass (m_0)
0.615	0.122	0.369	0.492
0.984	0.098	0.738	0.250
1.353	0.085	1.107	0.183
1.722	0.077	1.476	0.138

Table 1. (a) Bandgap energy v/s Width for family N= 3p+1, where p lies in [1, 4], (b) Bandgap energy v/s Width for family N= 3p+2, where p lies in [1, 4], (c) Bandgap energy v/s Width for family N= 3p, where p lies in [2, 5]

a		b		c	
Width W (nm)	Bandgap energy (eV)	Width W (nm)	Bandgap energy (eV)	Width W (nm)	Bandgap energy (eV)
0.369	2.80490	0.492	0.34921	0.615	1.24090
0.738	1.70610	0.861	0.23042	0.984	0.87405
1.107	1.22370	1.230	0.17193	1.353	0.67445
1.476	0.95346	1.599	0.13712	1.722	0.54903

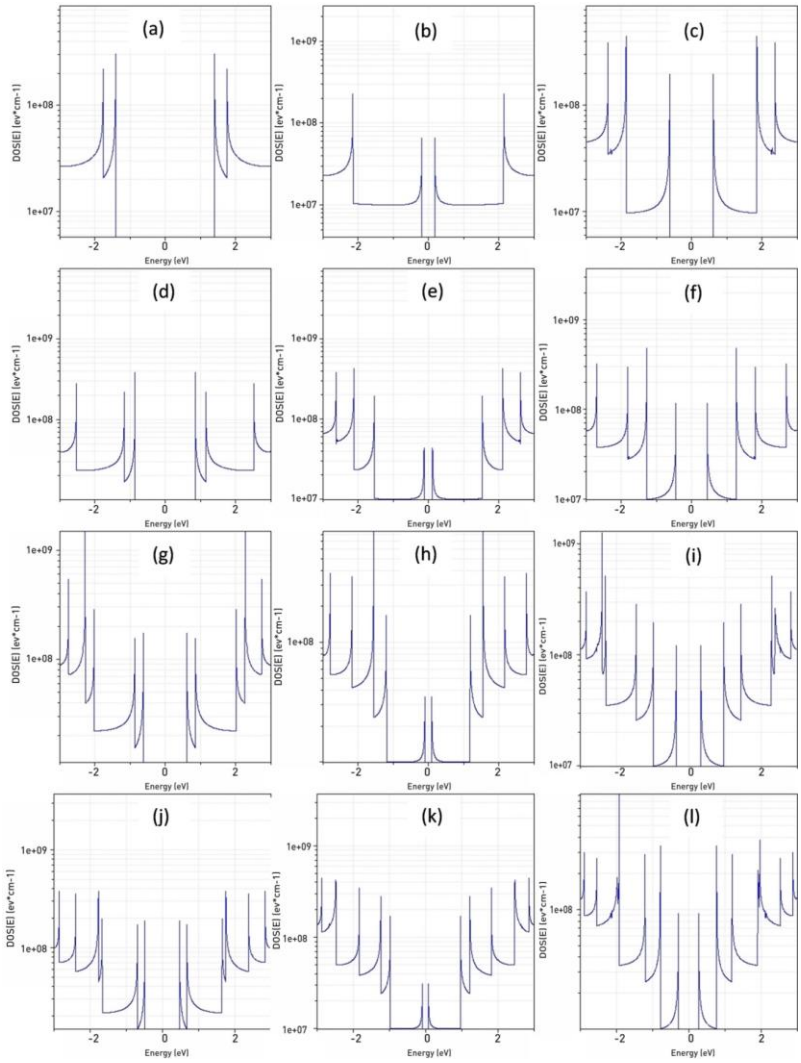

Figure 5. Density of States of AGNR. (a) N=4. (b) N=5. (c) N=6. (d) N=7. (e) N=8. (f) N=9. (g) N=10. (h) N=11. (i) N=12. (j) N=13. (k) N=14. (l) N=15

So obtained energy dispersion relation gives rise to the density of states that varies as $E^{-½}$. The gap opening in the density of states determines the energy gap. Symmetrical behavior is observed in several states in the valence band and the conduction band. Taking into account the fact that GNR comprises of sp^2 bonding and the π bonding, it can be inferred that p-shell is mainly responsible for the states near the Fermi level this is following the findings of Chang et al (Fan & Chang 2017).

4. Conclusions

Tight binding model π electron approximation has been employed to investigate the structural aspects, electronic band structure, and effective mass of AGNR for different chirality. The simulation reveals that AGNR in some cases has metallic nature while in other cases it behaves like a semiconductor. The armchair edge GNR belonging to family N = 3p and 3p+1 are perfect semiconductors, whereas the armchair edge GNR of family 3p+2 are metallic, and have a very narrow bandgap. N refers to the number of pairs of atoms per GNR unit cell termed as dimer lines. The density of states study variation with energy also confirms the existence of bandgap in AGNR. The bandgap varies with ribbon width due to quantum confinement. Finally, the study of variation of the effective mass m^* of charge carrier with width has shown that m^* decreases as the ribbon width of the GNR increases.

References

Borin Barin, G., Fairbrother, A., Rotach, L., Bayle, M., Paillet, M., Liang, L., . . . Ruffieux, P. (2019). Surface-synthesized graphene nanoribbons for room temperature switching devices: substrate transfer and ex situ characterization. *ACS applied nano materials*, *2*(4), 2184-2192. doi:10.1021/acsanm.9b00151

Cassiano, T. D. S. A., Monteiro, F. F., de Sousa, L. E., e Silva, G. M., & de Oliveira Neto, P. H. (2020). Smooth gap tuning strategy for cove-type graphene nanoribbons. *RSC Advances*, *10*(45), 26937-26943. doi:10.1039/D0RA02997A

Chen, Y. Y., Sangai, A., Gholipour, M., & Chen, D. (2013, September). Graphene nano-ribbon field-effect transistors as future low-power devices. *International Symposium on Low Power Electronics and Design (ISLPED)* (pp. 151-156). IEEE. doi: 10.1109/ISLPED.2013.6629286

Cui, L., Wang, J., & Sun, M. (2021). Graphene plasmon for optoelectronics. *Reviews in Physics*, 100054. doi:10.1016/j.revip.2021.100054

Dubois, S. M., Zanolli, Z., Declerck, X., & Charlier, J. C. (2009). Electronic properties and quantum transport in Graphene-based nanostructures. *The European Physical Journal B*, *72*(1), 1-24. doi:10.1140/epjb/e2009-00327-8

Fan, B., & Chang, S. (2017). Confined state energies in AGNR semiconductor–semiconductor hetero structure. *Physics Letters A*, *381*(4), 319-322. doi: 10.1016/j.physleta.2016.11.004

Ghosh, D., Sarkar, K., Devi, P., Kim, K. H., & Kumar, P. (2021). Current and future perspectives of carbon and graphene quantum dots: From synthesis to strategy for building optoelectronic and energy devices. *Renewable and Sustainable Energy Reviews*, *135*, 110391. doi:10.1016/j.rser.2020.110391

Goringe, C. M., Bowler, D. R., & Hernandez, E. (1997). Tight-binding modelling of materials. *Reports on Progress in Physics*, *60*(12), 1447. doi:10.1088/0034-4885/60/12/001

Hayyu, A. R., Azhar, A., & Majidi, M. A. (2018, October). Study of band structure renormalization of tight-binding model semiconductor by incorporating GW self-energy. *AIP Conference Proceedings* (Vol. 2023, No. 1, p. 020053). doi:10.1063/1.5064050

Houtsma, R. K., de la Rie, J., & Stöhr, M. (2021). Atomically precise graphene nanoribbons: interplay of structural and electronic properties. *Chemical Society Reviews*. doi: 10.1039/D0CS01541E

Jaramillo-Quintero, O. A., Barrera-Peralta, R. V., El Hachimi, A. G., Guillén-López, A., Pérez, O., Reguera, E., . . . Muñiz, J. (2021). Understanding the interaction between heteroatom-doped carbon matrix and Sb2S3 for efficient sodium-ion battery anodes. *Journal of Colloid and Interface Science*, *585*, 649-659. doi: 10.1016/j.jcis.2020.10.044

Jhamb, R., Kamal, D., Randhawa, K., & Sharma, A (2015). Theoretical Investigation of Electronic Properties of Armchair Graphene Nanoribbon. *Journal of Material Science and Mechanical Engineering.*

Jia, T. T., Zheng, M. M., Fan, X. Y., Su, Y., Li, S. J., Liu, H. Y., . . . Kawazoe, Y. (2016). Dirac cone move and bandgap on/off switching of graphene superlattice. *Scientific reports*, *6*(1), 1-11. doi:10.1038/srep18869

Johari, Z., Ahmadi, M. T., Chek, D. C. Y., Amin, N. A., & Ismail, R. (2010). Modelling of graphene nanoribbon Fermi energy. *Journal of Nanomaterials*, *2010*. doi:10.1155/2010/909347

Jun, Y. S., Habibpour, S., Hamidinejad, M., Park, M. G., Ahn, W., Yu, A., & Park, C. B. (2021). Enhanced electrical and mechanical properties of graphene nano-ribbon/thermoplastic polyurethane composites. *Carbon*, *174*, 305-316. doi: 10.1016/j.carbon.2020.12.023

Kheirabadi, S. J., Ghayour, R., & Sanaee, M. (2020). Negative differential resistance effect in different structures of armchair graphene nanoribbon. *Diamond and Related Materials*, *108*, 107970. doi:10.1016/j.diamond.2020.107970

Kim, J., Lee, N., Min, Y. H., Noh, S., Kim, N. K., Jung, S., . . . Yamada, Y. (2018). Distinguishing zigzag and armchair edges on graphene nanoribbons by X-ray photoelectron and Raman spectroscopies. *ACS Omega*, *3*(12), 17789-17796. doi:10.1021/acsomega.8b02744

Knoch, J. (2020). *Nanoelectronics: Device physics, fabrication, simulation*. Berlin, Germany: Walter de Gruyter.

Kuzmany, H., Shi, L., Martinati, M., Cambré, S., Wenseleers, W., Kürti, J., . . . Pichler, T. (2021). Well-defined sub-nanometer graphene ribbons synthesized inside carbon nanotubes. *Carbon*, *171*, 221-229. doi:10.1016/j.carbon.2020.08.065

Li, H., Xu, C., Srivastava, N., & Banerjee, K. (2009). Carbon nanomaterials for next-generation interconnects and passives: physics, status, and prospects. *IEEE Transactions on Electron Devices*, *56*(9), 1799-1821. doi:10.1109/TED.2009.2026524

Ma, F., Guo, Z., Xu, K., & Chu, P. K. (2012). First-principle study of energy band structure of armchair graphene nanoribbons. *Solid state communications*, *152*(13), 1089-1093. doi:10.1016/j.ssc.2012.04.058

Miyake, T., & Saito, S. (2005). Band-gap formation in (n, 0) single-walled carbon nanotubes (n= 9, 12, 15, 18): A first-principles study. *Physical Review B*, *72*(7), 073404. doi: 10.1103/PhysRevB.72.073404

Mu, X., & Sun, M. (2020). The linear and non-linear optical absorption and asymmetrical electromagnetic interaction in chiral twisted bilayer graphene with hybrid edges. *Materials Today Physics*, *14*, 100222. doi:10.1016/j.mtphys.2020.100222

Mu, X., Chai, J., Wang, J., Li, Y., & Sun, M. (2019). Physical mechanism on edge-dependent electrons transfer in graphene in mid infrared region. *Spectrochimica Acta Part A: Molecular and Biomolecular Spectroscopy*, *216*, 136-145. doi:10.1016/j.saa.2019.03.024

Nakada, K., Fujita, M., Dresselhaus, G., & Dresselhaus, M. S. (1996). Edge state in graphene ribbons: Nanometer size effect and edge shape dependence. *Physical Review B*, *54*(24), 17954. doi:10.1103/PhysRevB.54.17954

Poklonski, N. A., Kislyakov, E. F., Vyrko, S. A., Bubel, O. N., & Ratkevich, S. V. (2012). Electronic band structure and magnetic states of zigzag graphene nanoribbons: quantum chemical calculations. *Journal of Nanophotonics*, *6*(1), 061712. doi: 10.1117/1.JNP.6.061712

Ray, B., Parmar, S., Date, K., & Datar, S. (2021). Optically transparent polymer composites: a study on the influence of filler/dopant on electromagnetic interference shielding mechanism. *Journal of Applied Polymer Science*, *138*(16), 50255. doi: 10.1002/app.50255

Raza, H., & Kan, E. C. (2008). Armchair graphene nanoribbons: Electronic structure and electric-field modulation. *Physical Review B*, *77*(24), 245434. doi: 10.1103/PhysRevB.77.245434

Sahu, S., & Rout, G. C. (2017). Band gap opening in graphene: a short theoretical study. *International Nano Letters*, *7*(2), 81-89. doi:10.1007/s40089-017-0203-5

Sako, R., Hosokawa, H., & Tsuchiya, H. (2010). Computational study of edge configuration and quantum confinement effects on graphene nanoribbon transport. *IEEE electron device letters*, *32*(1), 6-8. doi:10.1109/LED.2010.2086426

Salih, E., & Ayesh, A. I. (2021). Pt-doped armchair graphene nanoribbon as a promising gas sensor for CO and CO2: DFT study. *Physica E: Low-dimensional Systems and Nanostructures*, *125*, 114418. doi:10.1016/j.physe.2020.114418

Senkovskiy, B. V., Nenashev, A. V., Alavi, S. K., Falke, Y., Hell, M., Bampoulis, P., . . . Grüneis, A. (2021). Tunneling current modulation in atomically precise graphene nanoribbon heterojunctions. *Nature Communications*, *12*(1), 1-11. doi:10.1038/s41467-021-22774-0

Seol, G., Yoon, Y., Fodor, J. K., Guo, J., Matsudaira, A., Kienle, D., . . . Saeed, A. I. (2006). CNTbands. doi:10.21981/QT2F-0B32

Sheka, E. F. (2018). Dirac material graphene. *Reviews on Advanced Materials Science*, *53*(1), 1-28. doi:10.1515/rams-2018-0001

Shekhirev, M., & Sinitskii, A. (2017). Solution synthesis of atomically precise graphene nanoribbons. *Physical Sciences Reviews*, *2*(5). doi:10.1515/psr-2016-0108

Shrivastav, A. M., Cvelbar, U., & Abdulhalim, I. (2021). A comprehensive review on plasmonic-based bio sensors used in viral diagnostics. *Communications Biology*, *4*(1), 1-12. doi:10.1038/s42003-020-01615-8

Son, Y. W., Cohen, M. L., & Louie, S. G. (2006). Energy gaps in graphene nanoribbons. *Physical Review Letters*, *97*(21), 216803. doi:10.1103/PhysRevLett.97.216803

Tayo, B. O. (2014). Effective mass versus band gap in graphene nanoribbons: influence of H-passivation and uniaxial strain. *Materials Focus*, *3*(4), 248-254. doi:10.1166/mat.2014.1182

Wakabayashi, K., Sasaki, K. I., Nakanishi, T., & Enoki, T. (2010). Electronic states of graphene nanoribbons and analytical solutions. *Science and Technology of Advanced Materials*. doi:10.1088/1468-6996/11/5/054504

Wang, J., Zhao, R., Yang, M., Liu, Z., & Liu, Z. (2013). Inverse relationship between carrier mobility and bandgap in graphene. *The Journal of Chemical Physics*, *138*(8), 084701. doi:10.1063/1.4792142

Wang, Z. F., Li, Q., Zheng, H., Ren, H., Su, H., Shi, Q. W., & Chen, J. (2007). Tuning the electronic structure of graphene nanoribbons through chemical edge modification: A theoretical study. *Physical Review B*, *75*(11), 113406. doi:10.1103/PhysRevB.75.113406

Wang, Z., Ye, S., Wang, H., He, J., Huang, Q., & Chang, S. (2021). Machine learning method for tight-binding Hamiltonian parameterization from ab-initio band structure. *npj Computational Materials*, *7*(1), 1-10. doi:10.1038/s41524-020-00490-5

Wieland, L., Li, H., Rust, C., Chen, J., & Flavel, B. S. (2021). Carbon nanotubes for photovoltaics: from lab to industry. *Advanced Energy Materials*, *11*(3), 2002ss880. doi:10.1002/aenm.202002880

Wilhelm, J., Golze, D., Talirz, L., Hutter, J., & Pignedoli, C. A. (2018). Toward GW calculations on thousands of atoms. *The Journal of Physical Chemistry Letters*, *9*(2), 306-312. doi:10.1021/acs.jpclett.7b02740

Xie, F., Fan, Z. Q., Liu, K., Wang, H. Y., Yu, J. H., & Chen, K. Q. (2015). Negative differential resistance and stable conductance switching behaviors of salicylideneaniline molecular devices sandwiched between armchair graphene nanoribbon electrodes. *Organic Electronics*, *27*, 41-45. doi:10.1016/j.orgel.2015.08.028

Yang, W., Lucotti, A., Tommasini, M., & Chalifoux, W. A. (2016). Bottom-up synthesis of soluble and narrow graphene nanoribbons using alkyne benzannu lations. *Journal of the American Chemical Society*, *138*(29), 9137-9144. doi:10.1021/jacs.6b03014

Yazyev, O. V. (2013). A guide to the design of electronic properties of graphene nanoribbons. *Accounts of Chemical Research*, *46*(10), 2319-2328. doi:10.1021/ar3001487